

Mass-Flux Budgets of Shallow Cumulus Clouds

STEPHAN R. DE ROODE AND CHRISTOPHER S. BRETHERTON

Department of Atmospheric Sciences, University of Washington, Seattle, Washington

(Manuscript received 21 September 2001, in final form 21 June 2002)

ABSTRACT

The vertical transport by shallow nonprecipitating cumulus clouds of conserved variables, such as the total specific humidity or the liquid water potential temperature, can be well modeled by the mass-flux approach, in which the cloud field is represented by a top-hat distribution of clouds and its environment. The mass-flux budget is computed by conditionally sampling the prognostic vertical velocity equation by means of a large eddy simulation of shallow cumulus clouds. The model initialization is based on observations made during the Barbados Oceanographic and Meteorological Experiment (BOMEX). Several different sampling criteria are applied. The presence of liquid water is used to select clouds, whereas additional criteria are applied to sample cloud updraft, downdraft, and core properties. A comparison between the budgets of the mass flux and the vertical velocity variance show that they appear to be qualitatively similar. The mass flux is driven by buoyancy in the lower part of the cloud layer, whereas turbulent transport is important in generating mass flux in the upper part of the cloud layer. Pressure and subgrid-scale effects typically act to dissipate mass flux. Entrainment and detrainment rates for the vertical velocity equation are presented. They are found to be smaller in comparison to the ones for conserved variables. It is explained that the top-hat structure for the virtual potential temperature is degraded by mixing at the cloud boundaries leading to a subsequent evaporative cooling of cloud droplets that supports the formation of negatively buoyant cloud parcels.

1. Introduction

The parameterization of vertical transport due to cumulus clouds is often performed by a mass-flux approach (Tiedtke 1989). In such schemes it is assumed that the cumulus cloud field can be well represented by a top-hat distribution. This decomposition requires a set of two separate prognostic equations that describe the (thermo)dynamical evolution of the clouds, and the surrounding environment. These two equations both include an entrainment and a detrainment term that represent the effect of lateral mixing of mass at the cloud interface (Stommel 1947; Arakawa and Schubert 1974; Tiedtke 1989; Siebesma and Holtslag 1996; Siebesma 1998). This parameterization of the net lateral exchange mirrors the idea that, if the velocity at the cloud boundary is pointed cloud inward, air properties of the environment are entrained by the cloud and vice versa. The lateral mixing rates to be used in a model can be based on observations (Nitta 1975; Raga et al. 1990) or from large eddy simulation (LES) results of shallow cumuli (Siebesma and Cuijpers 1995; Grant and Brown 1999; Stevens et al. 2001).

In addition to the lateral mixing rates, the cloud fraction and the convective mass flux need to be parameterized. The latter is usually diagnosed from the continuity equation for mass. The system can be then closed by either diagnosing or predicting the cloud fraction. LES-based studies of shallow cumuli have shown that, with suitable entrainment and detrainment rates, a mass-flux decomposition can represent quite well the vertical fluxes of conserved thermodynamic variables (Siebesma and Cuijpers 1995).

Instead of using the continuity equation for mass to diagnose the mass flux, some mass-flux-based cumulus parameterizations prognose the vertical velocity or the mass flux in the cloud (Asai and Kasahara 1967; Holton 1973; Cotton 1975; Lappen and Randall 2001a,b,c). This approach adds some more unknowns to solve since it requires the consideration of, for example, pressure and buoyancy effects. In view of the utility of a vertical velocity equation, one of our main goals in this paper is to investigate how well the mass-flux decomposition can represent the vertical velocity variance budget in LES of shallow cumuli. Moreover, we will analyze the budgets of the conditionally sampled vertical velocity and the mass flux.

In section 2, we present the conditionally sampled budget equations for the vertical velocity (Young 1988b; Schumann and Moeng 1991a,b), the mass flux, and the vertical velocity variance. In section 3, we summarize the LES of trade cumuli during BOMEX (the Barbados

Corresponding author address: Stephan R. de Roode, Institute for Marine and Atmospheric Research Utrecht, Faculteit Natuur-en Sterrenkunde, Universiteit van Utrecht, Princetonplein 5, 3584 CC Utrecht, Netherlands.
E-mail: roode@phys.uu.nl

TABLE 1. Summary of sampling criteria: $\overline{\theta}_v$ is the horizontal mean value of the virtual potential temperature and q_l is the liquid water content.

Indicator function	Type	Sampling criteria
I_0	Slab mean	None
I_1	Updraft	$w > 0$
I_2	Cloud	$q_l > 0$
I_3	Cloud updraft	$q_l > 0$ and $w > 0$
I_4	Cloud downdraft	$q_l > 0$ and $w < 0$
I_5	Cloud core	$q_l > 0$ and $w > 0$ and $\theta_v > \overline{\theta}_v$

Oceanographic and Meteorological Experiment in June 1969), which we use to analyze these budgets. In section 4, we present the conditionally sampled mass-flux budgets for various sampling criteria defining the active clouds, and compare them with Reynolds-averaged variance budgets. In section 5 we analyze reasons for the poor performance of the top-hat (mass flux) approximation in explaining the buoyancy flux and vertical velocity variance. Conclusions follow in section 6.

2. The conditionally sampled vertical velocity equation

a. LES model equations

In our simulations and analyses, we use the Boussinesq equations and their LES implementation. The filtered prognostic equations for the resolved part of an arbitrary conserved variable ψ and the Boussinesq form of the momentum equation read, respectively,

$$\frac{\partial \psi}{\partial t} = -\frac{\partial u_j \psi}{\partial x_j} - \frac{\partial \overline{u_j'' \psi''}}{\partial x_j} + S_\psi, \quad (1)$$

$$\frac{\partial u_i}{\partial t} = \frac{g}{\theta_0}(\theta_v - \overline{\theta}_v)\delta_{i3} - \frac{\partial u_i u_j}{\partial x_j} - \frac{\partial \pi}{\partial x_i} - \frac{\partial \tau_{ij}}{\partial x_j}. \quad (2)$$

The variable ψ represents the total water specific humidity q_t or the liquid water potential temperature θ_l ; S_ψ is a source term that can represent processes like radiation or precipitation. The velocity components $u_i = (u, v, w)$ are the components in $x_i = (x, y, z)$ directions, respectively; π is the modified pressure (Deardorff 1973); t is the time; g the gravitational acceleration; $\theta_v - \overline{\theta}_v$ the perturbation of the virtual potential temperature with respect to its horizontally averaged mean value; θ_0 the reference-state potential temperature; δ_{ij} the Kronecker delta; and $\overline{u_j'' \psi''}$ and τ_{ij} are the subgrid flux terms that arise from the filtering procedure. In the LES model the latter are expressed as the product of an eddy viscosity K_m or eddy diffusivity K_ψ and the local gradient of the resolved variable:

$$\overline{u_j'' \psi''} = -K_\psi \frac{\partial \psi}{\partial x_j}, \quad (3)$$

$$\tau_{ij} = -K_m \left(\frac{\partial u_i}{\partial x_j} + \frac{\partial u_j}{\partial x_i} \right). \quad (4)$$

b. Conditional sampling technique

The conditionally sampled mean value $[\psi]_s$ is defined as

$$[\psi]_s = \frac{\int_A I_s \psi \, dA}{\int_A I_s \, dA}, \quad (5)$$

where the integration is performed over a horizontal plane at height z and I_s is an indicator function: $I_s = 1$ if a sampling criterion is met, and $I_s = 0$ otherwise. In the LES model the integrals are evaluated by a summation over discrete grid points (Schumann and Moeng 1991a,b). To determine properties of the cumulus clouds only, one usually samples on the presence of liquid water (q_l), although several other criteria are sometimes added. For instance, the cloud core is defined as the part of the cloud that has both an upward vertical velocity and a positive virtual potential temperature excess. The sampling criteria that have been applied are summarized in Table 1. The sampled area fraction σ_s is defined as

$$\sigma_s = \frac{\int_A I_s \, dA}{\int_A dA}. \quad (6)$$

For a two-stream approximation we can define the fraction of the environment σ_e as

$$\sigma_e = 1 - \sigma_s. \quad (7)$$

By this definition the environment represents the area fraction of all points where the applied sampling criterion is not satisfied. In the remainder of the paper the square brackets that indicate the conditionally sampled mean are, for notational convenience, omitted except when the operator is applied on a derivative. The horizontal slab-mean value is indicated by an overbar and is given by

$$\overline{\psi} = \sigma_s \psi_s + (1 - \sigma_s) \psi_e. \quad (8)$$

We define the mass flux M_c as

$$M_c \equiv \sigma_s (w_s - \overline{w}) = \sigma_s (1 - \sigma_s) (w_s - w_e), \quad (9)$$

which has, for notational convenience, units of meters per second. The continuity equation for mass is given by

$$\frac{\partial M_c}{\partial z} = -\frac{\partial \sigma}{\partial t} + E - D, \quad (10)$$

with E and D the lateral entrainment and detrainment rates, respectively. The Reynolds-averaged covariance $\overline{w' \psi'}$ is related to mass-flux variables as (Siebesma and Cuijpers 1995)

$$\begin{aligned}\overline{w'\psi'} &= \sigma_s[w'\psi']_s + (1 - \sigma_s)[w'\psi']_e \\ &= \sigma_s(1 - \sigma_s)(w_s - w_e)(\psi_s - \psi_e) \\ &\quad + \sigma_s[w''\psi'']_s + (1 - \sigma_s)[w''\psi'']_e,\end{aligned}\quad (11)$$

where the latter two terms indicate the so-called subplume fluxes, which are due to the contributions of perturbations with respect to the conditionally sampled mean. We distinguish second-order moments in the top-hat (mass flux) approach by a subscript MF. In this notation, the vertical flux ($w'\psi'_{\text{MF}}$), the variance ($\psi'\psi'_{\text{MF}}$), and their relation to the Reynolds-averaged statistics read

$$\begin{aligned}\overline{w'\psi'_{\text{MF}}} &= \sigma_s(1 - \sigma_s)(w_s - w_e)(\psi_s - \psi_e) \\ &= \kappa_{w\psi}\overline{w'\psi'},\end{aligned}\quad (12)$$

$$\overline{\psi'\psi'_{\text{MF}}} = \sigma_s(1 - \sigma_s)(\psi_s - \psi_e)^2 = \kappa_{\psi\psi}\overline{\psi'\psi'}.\quad (13)$$

The factors $\kappa_{w\psi}$ and $\kappa_{\psi\psi}$ are a measure for the representativity of the top-hat approach for the Reynolds-averaged second-order moments. For a cumulus cloud field the factor $\kappa_{w\psi}$ is close to one (Siebesma and Cuijpers 1995), indicating that the top-hat flux represents the Reynolds-averaged flux of a conserved variable rather well. In that case the subplume contribution is very small. For stratocumulus and the clear convective boundary layer $\kappa_{w\psi}$ has an approximate value of 0.6 (Schumann and Moeng 1991b; Wyngaard and Moeng 1992; Young 1988a; de Laat and Duynkerke 1998). In general, the top-hat approximation is less well capable to represent $\psi'\psi'$ (Wang and Stevens 2000).

c. The conditionally sampled prognostic vertical velocity equation

Conditionally sampling Eq. (2) for the vertical velocity gives

$$\begin{aligned}\left[\frac{\partial w}{\partial t}\right]_s &= \frac{g}{\theta_0}(\theta_{v,s} - \overline{\theta}_v) - \left[\frac{\partial w^2}{\partial z}\right]_s - \left[\frac{\partial u_h w}{\partial x_h}\right]_s \\ &\quad - \left[\frac{\partial \pi}{\partial z}\right]_s - \left[\frac{\partial \tau_{3j}}{\partial x_j}\right]_s,\end{aligned}\quad (14)$$

where $u_h = (u, v)$ and $\partial x_h = (\partial x, \partial y)$.

If the sampling operator is moved inside a derivative, two additional terms arise due to the chain rule of differentiation and the application of Leibniz' rule (Young 1988b; Schumann and Moeng 1991a). The conditionally sampled time derivative of the vertical velocity, for example, is then given by

$$\left[\frac{\partial w}{\partial t}\right]_s = \frac{\partial w_s}{\partial t} + \frac{w_s}{\sigma_s} \frac{\partial \sigma_s}{\partial t} + \left\{ \frac{\partial w}{\partial t} \right\}_{b,s},\quad (15)$$

where we used the braces with subscript b,s to indicate the net effect of the boundary terms that follow from Leibniz' rule. To calculate the term in braces one needs to track the evolution of the cloud boundaries. However, one can avoid this laborious exercise by computing the other three terms in (15). Similarly, the second term on the rhs. of (14) can be rewritten

$$\left[\frac{\partial w^2}{\partial z}\right]_s = \frac{\partial [w^2]_s}{\partial z} + \frac{[w^2]_s}{\sigma_s} \frac{\partial \sigma_s}{\partial z} + \left\{ \frac{\partial w^2}{\partial z} \right\}_{b,s}.\quad (16)$$

1) THE PROGNOSTIC MASS-FLUX EQUATION

An identical equation to (14) can be written for the environment simply by replacing the subscript s with e . If we multiply Eq. (14) times a factor $\sigma_s(1 - \sigma_s)$ and subtract the conditionally sampled prognostic vertical velocity equation for the environment multiplied times the same factor, we obtain

$$\begin{aligned}\frac{\partial M_c}{\partial t} + \sigma_s(1 - \sigma_s) \left(\left\{ \frac{\partial w}{\partial t} \right\}_{b,s} - \left\{ \frac{\partial w}{\partial t} \right\}_{b,e} \right) \\ = \sigma_s(1 - \sigma_s) \frac{g}{\theta_0} (\theta_{v,s} - \theta_{v,e}) - \sigma_s(1 - \sigma_s) \left(\left[\frac{\partial w^2}{\partial z} \right]_s - \left[\frac{\partial w^2}{\partial z} \right]_e \right) \\ - \sigma_s(1 - \sigma_s) \left(\left[\frac{\partial u_h w}{\partial x_h} \right]_s - \left[\frac{\partial u_h w}{\partial x_h} \right]_e \right) - \sigma_s(1 - \sigma_s) \left(\left[\frac{\partial \pi}{\partial z} \right]_s - \left[\frac{\partial \pi}{\partial z} \right]_e \right) - \sigma_s(1 - \sigma_s) \left(\left[\frac{\partial \tau_{3j}}{\partial x_j} \right]_s - \left[\frac{\partial \tau_{3j}}{\partial x_j} \right]_e \right),\end{aligned}\quad (17)$$

where we used (8), (9), and (15) to obtain the tendency of the mass flux:

$$\begin{aligned}\sigma_s(1 - \sigma_s) \left(\left[\frac{\partial w}{\partial t} \right]_s - \left[\frac{\partial w}{\partial t} \right]_e \right) &= (1 - \sigma_s) \frac{\partial \sigma_s w_s}{\partial t} - \sigma_s \frac{\partial (1 - \sigma_s) w_e}{\partial t} + \sigma_s(1 - \sigma_s) \left(\left\{ \frac{\partial w}{\partial t} \right\}_{b,s} - \left\{ \frac{\partial w}{\partial t} \right\}_{b,e} \right) \\ &= \frac{\partial M_c}{\partial t} + \overline{w} \frac{\partial \sigma_s}{\partial t} + \sigma_s(1 - \sigma_s) \left(\left\{ \frac{\partial w}{\partial t} \right\}_{b,s} - \left\{ \frac{\partial w}{\partial t} \right\}_{b,e} \right).\end{aligned}\quad (18)$$

Note that we neglect the effect of the mean vertical velocity term (\bar{w}) in the prognostic mass-flux equation (17) and the second-order moment equations.

2) ENTRAINMENT AND DETRAINMENT

Siebesma and Cuijpers (1995) computed the lateral entrainment and detrainment rates by a careful analysis of the budget equation for conserved variables:

$$\frac{\partial \sigma_s \psi_s}{\partial t} = -\frac{\partial M_c \psi_s}{\partial z} - \frac{\partial \sigma_s [w'' \psi'']_s}{\partial z} + E \psi_e - D \psi_s + \sigma S_{\psi_s}. \quad (19)$$

Likewise, we can express a similar equation for the conditionally sampled vertical velocity:

$$\frac{\partial \sigma_s w_s}{\partial t} = -\frac{\partial M_c w_s}{\partial z} - \frac{\partial \sigma_s [w'' w'']_s}{\partial z} + E_w w_e - D_w w_s + \sigma_s S_{w_s}, \quad (20)$$

with E_w and D_w representing the entrainment and detrainment rates to be diagnosed from the vertical velocity equation. The source function S_{w_s} comprises the buoyancy and the pressure terms:

$$S_{w_s} = \frac{g}{\theta_0} (\theta_{v,s} - \bar{\theta}_v) - \left[\frac{\partial \pi}{\partial z} \right]_s. \quad (21)$$

After comparing (14) multiplied times σ_s to (20) and considering (15) and (16) it follows that the total lateral exchange term is given by

$$E_w w_e - D_w w_s = -\sigma_s \left[\frac{\partial u_h w}{\partial x_h} \right]_s - \sigma_s \left[\frac{\partial \tau_{3j}}{\partial x_j} \right]_s - \sigma_s \left\{ \frac{\partial w}{\partial t} \right\}_{b,s} - \sigma_s \left\{ \frac{\partial w^2}{\partial z} \right\}_{b,s}. \quad (22)$$

If we require that the continuity equation must be satisfied,

$$\frac{\partial M_c}{\partial z} = -\frac{\partial \sigma_s}{\partial t} + E_w - D_w; \quad (23)$$

E_w and D_w can be obtained from (22) and (23).

3) THE VERTICAL VELOCITY VARIANCE EQUATION

In order to derive a prognostic equation for the vertical velocity variance in the mass-flux approach we will use as starting equations (20) multiplied times $(1 - \sigma_s)$ and the analogous equation for the vertical velocity in the environment multiplied times a factor σ_s ,

$$(1 - \sigma_s) \frac{\partial \sigma_s w_s}{\partial t} = -(1 - \sigma_s) \frac{\partial M_c w_s}{\partial z} - (1 - \sigma_s) \frac{\partial \sigma_s [w'' w'']_s}{\partial z} + (1 - \sigma_s) (E_w w_e - D_w w_s) + \sigma_s (1 - \sigma_s) S_{w_s}, \quad (24)$$

$$\begin{aligned} \sigma_s \frac{\partial (1 - \sigma_s) w_e}{\partial t} &= \sigma_s \frac{\partial M_c w_e}{\partial z} - \sigma_s \frac{\partial (1 - \sigma_s) [w'' w'']_e}{\partial z} \\ &\quad - \sigma_s (E_w w_e - D_w w_s) + \sigma_s (1 - \sigma_s) S_{w_e}. \end{aligned} \quad (25)$$

After multiplying (24) and (25) times $2(w_s - w_e)$ and some mathematical manipulations according to the procedure presented by de Roode et al. (2000) we obtain

$$\begin{aligned} \frac{\partial \sigma_s (1 - \sigma_s) (w_s - w_e)^2}{\partial t} &= 2 \frac{g}{\theta_0} M_c (\theta_{v,s} - \theta_{v,e}) - \frac{\partial (1 - 2\sigma_s) M_c (w_s - w_e)^2}{\partial z} \\ &\quad - 2M_c \left(\frac{1}{\sigma_s} \frac{\partial \sigma_s [w'' w'']_s}{\partial z} - \frac{1}{1 - \sigma_s} \frac{\partial (1 - \sigma_s) [w'' w'']_e}{\partial z} \right) - 2M_c \left(\left[\frac{\partial \pi}{\partial z} \right]_s - \left[\frac{\partial \pi}{\partial z} \right]_e \right) \\ &\quad - (E_w + D_w) (w_s - w_e)^2 + R \end{aligned} \quad (26)$$

with the residual R ,

$$R = -(1 - 2\sigma_s) (w_s - w_e)^2 \frac{\partial \sigma_s}{\partial t}, \quad (27)$$

where we neglect terms including the mean vertical velocity, but unlike de Roode et al. (2000) we do not assume $\partial \sigma_s / \partial t = 0$.

In the Reynolds-averaging approach the vertical velocity variance budget equation reads (Stull 1988)

$$\frac{\partial \overline{w'^2}}{\partial t} = 2 \frac{g}{\theta_0} \overline{w' \theta'_v} - \frac{\partial \overline{w'^3}}{\partial z} - 2 \overline{w' \frac{\partial \pi'}{\partial z}} - 2 \overline{w' \frac{\partial \tau'_{3j}}{\partial x_j}}, \quad (28)$$

where the primes indicate perturbations of the resolved variables with respect to the horizontal slab-mean value. By (12) and (13), the correspondence between the vertical velocity variance tendency, the buoyancy flux, and the pressure term in (26) and (28) is obvious. The dissipation of the vertical velocity variance in (26) is rep-

TABLE 2. Summary of the terms in the vertical velocity variance, mass flux, and conditionally sampled vertical velocity budgets.

Term	$\overline{w'w'}$ budget	M_c budget	w_s budget
Tendency	$\frac{\partial \overline{w'^2}}{\partial t}$	$\frac{\partial M_c}{\partial t} + \sigma_s(1 - \sigma_s) \left(\left[\frac{\partial w}{\partial t} \right]_{b,s} - \left[\frac{\partial w}{\partial t} \right]_{b,e} \right)$	$\frac{\partial w_s}{\partial t} + \frac{w_s}{\sigma_s} \frac{\partial \sigma_s}{\partial t} + \left[\frac{\partial w}{\partial t} \right]_{b,s}$
Buoyancy	$2 \frac{g}{\theta_0} \overline{w'\theta'_v}$	$\frac{g}{\theta_0} \sigma_s(1 - \sigma_s)(\theta_{v,s} - \theta_{v,e})$	$\frac{g}{\theta_0}(\theta_{v,s} - \theta_{v,e})$
Pressure	$-2 \overline{w' \frac{\partial \pi'}{\partial z}}$	$-\sigma_s(1 - \sigma_s) \left(\left[\frac{\partial \pi}{\partial z} \right]_s - \left[\frac{\partial \pi}{\partial z} \right]_e \right)$	$-\left[\frac{\partial \pi}{\partial z} \right]_s$
Turbulent transport	$-\frac{\partial \overline{w'^3}}{\partial z}$	$-\sigma_s(1 - \sigma_s) \left(\left[\frac{\partial w^2}{\partial z} \right]_s - \left[\frac{\partial w^2}{\partial z} \right]_e \right)$	$-\frac{\partial [w^2]_s}{\partial z} - \frac{[w^2]_s}{\sigma_s} \frac{\partial \sigma_s}{\partial z} - \left[\frac{\partial w^2}{\partial z} \right]_{b,s}$
Subgrid dissipation	$-2 \overline{w' \frac{\partial \tau'_{3j}}{\partial x_j}}$	$-\sigma_s(1 - \sigma_s) \left(\left[\frac{\partial \tau_{3j}}{\partial x_j} \right]_s - \left[\frac{\partial \tau_{3j}}{\partial x_j} \right]_e \right)$	$-\left[\frac{\partial \tau_{3j}}{\partial z} \right]_s$
Lateral exchange	—	$-\sigma_s(1 - \sigma_s) \left(\left[\frac{\partial u_s w}{\partial z} \right]_s - \left[\frac{\partial u_s w}{\partial z} \right]_e \right)$	$-\left[\frac{\partial u_s w}{\partial z} \right]_s$

resented by the term that includes the lateral mixing rates. Moreover, Randall et al. (1992) showed that for a top-hat distribution the turbulent transport term is given by

$$\overline{w'^3}_{MF} = (1 - 2\sigma_s)M_c(w_s - w_e)^2. \quad (29)$$

Table 2 summarizes the components of the budget equations for the vertical velocity variance, mass flux, and the conditionally sampled vertical velocity w_s .

3. Large eddy simulation of the BOMEX case

a. Experimental setup

The large eddy simulation has been performed with the Institute for Marine and Atmospheric Research, Utrecht/Royal Netherlands Meteorological Institute (IMAU/KNMI) model (Cuijpers 1994; Siebesma and Cuijpers 1995; VanZanten 2000). The simulation was done with a central-difference scheme ($64 \times 64 \times 75$ points). The horizontal and vertical grid spacings were

100 m and 40 m, respectively. The initialization was based on the BOMEX field experiment. We performed a simulation of 6 hours, and used the results of the last 4 hours for our analysis by averaging over all output fields during this time period. Since only a few clouds penetrate the inversion layer above 1500 m, the statistics in this layer are very poor and are therefore not discussed. The initialization and large-scale forcings are described in detail by Siebesma and Cuijpers (1995) and a follow-up study by the participants of the GEWEX (Global Water and Energy Experiment), Cloud Systems Study Working Group 1.

b. The vertical velocity variance budget

To illustrate the dynamics of shallow cumulus clouds, the budget for the vertical velocity variance $\overline{w'^2}$, computed according to (28), is shown in Fig. 1. The buoyancy flux is the primary production source of $\overline{w'^2}$. Except for a shallow layer around the cloud base the buoy-

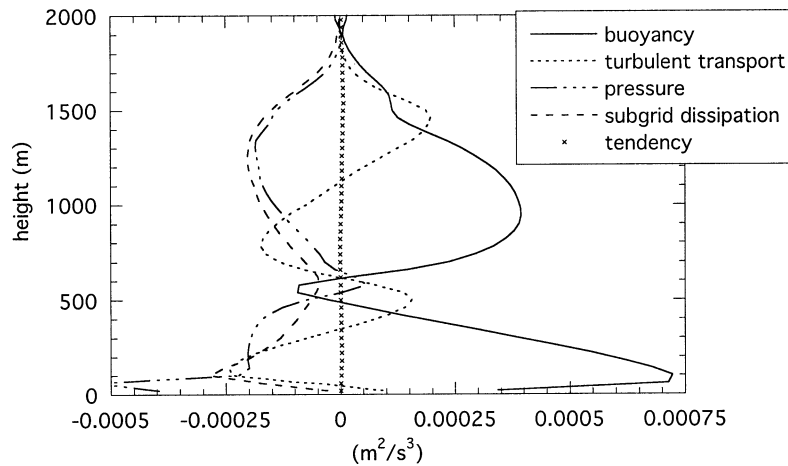


FIG. 1. The vertical velocity variance budget. Line styles are according to the legend.

ancy flux is positive from the surface up to the inversion layer. At the top of the mixed layer, where the buoyancy flux is negative, saturated air parcels can reach their level of free convection by the upward vertical momentum they have gained. At these levels the turbulence transport term is the major term that is producing vertical velocity variance. In addition, the pressure term gives a positive, albeit small contribution, near the cloud base as well. The turbulent transport term becomes positive above about 1100 m. In the bulk of the cloud layer the dissipation and the pressure gradient term act to destroy vertical velocity variance. The pressure term redistributes vertical momentum into the horizontal directions, whereas the dissipation of the resolved vertical motions produces subgrid-scale turbulence motions. Cuijpers et al. (1996) showed vertical velocity variance budgets for shallow cumuli from LES model results based on observations in Puerto Rico and during the Atlantic Trade Wind Experiment (ATEX). These budgets are qualitatively similar to the one from BOMEX. However, Cuijpers et al. showed that in the cloud layer the dissipation is considerably less negative than the pressure term, whereas during BOMEX they are nearly as important. This implies that the vertical velocity variance budget in shallow cumuli does not scale universally, which is a typical characteristic for cloudy boundary layers.

c. The variance budget for the liquid water potential temperature

De Roode et al. (2000) showed that the budget equation for the variance of a conserved variable in the mass-flux approach (13) reads

$$\begin{aligned} \frac{\partial \sigma_s (1 - \sigma_s) (\psi_s - \psi_e)^2}{\partial t} &= -2M_c (\psi_s - \psi_e) \frac{\partial \bar{\psi}}{\partial z} \\ &\quad - \frac{\partial (1 - 2\sigma_s) M_c (\psi_s - \psi_e)^2}{\partial z} \\ &\quad - (E + D) (\psi_s - \psi_e)^2. \end{aligned} \quad (30)$$

After comparing (30) with the Reynolds-averaged variance budget equation,

$$\frac{\partial \overline{\psi'^2}}{\partial t} = -2 \overline{w' \psi'} \frac{\partial \bar{\psi}}{\partial z} - \frac{\partial \overline{w' \psi' \psi'}}{\partial z} - 2\epsilon_\psi, \quad (31)$$

they concluded that the sum of the lateral mixing rates $E + D$, can be interpreted as an inverse dissipation timescale. They found that for a dry convective boundary layer these two budgets were very similar. As another example, we show the variance budgets for the liquid water potential temperature variance (θ'^2) for the BOMEX cumulus case in Fig. 2. It is clear that the bulk features of the two variance budgets are nearly the same. As inspection of the variance production term immediately makes clear that the fundamental mass-flux relation on which the top-hat approximation is based is

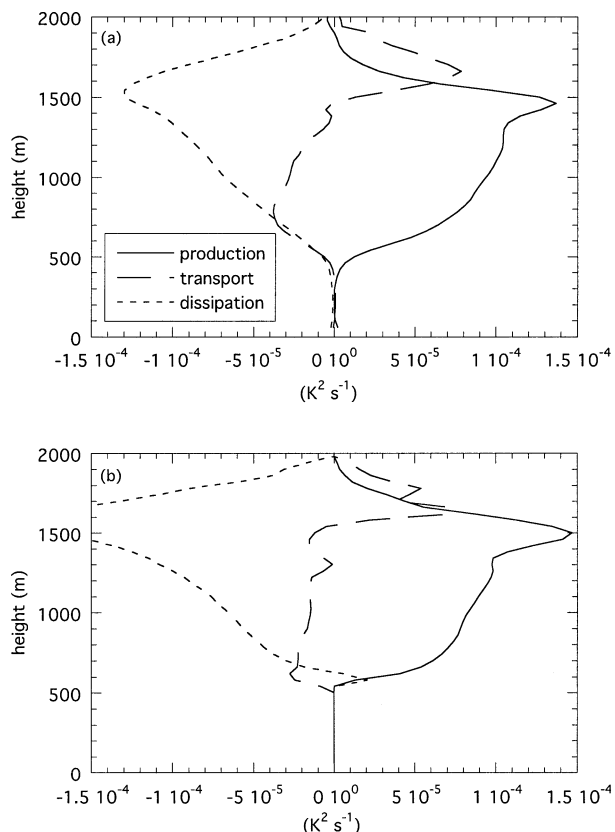


FIG. 2. The variance budgets for the liquid water potential temperature. (a) Reynolds-averaged equations. (b) Mass-flux approach for the cloud-environment decomposition. Line styles are according to the legend shown in (a).

satisfied, namely that the subplume contributions in (11) are negligibly small for the vertical flux of a conserved variable. Moreover, the main conclusion of de Roode et al. that parameterizing the dissipation term in the Reynolds variance budget is analogous to parameterizing E and D in the mass-flux equations is also supported by the budgets for cumulus clouds.

These findings raise the question whether similar results also hold for the vertical velocity equation. The next section therefore compares the Reynolds-averaged vertical velocity variance budget (28) shown in Fig. 1 to the one according to the mass-flux approach (26).

4. Conditionally sampled vertical velocity budgets

a. The mass-flux budget

The mass-flux budgets as computed according to Eq. (17) are shown in Fig. 3. They have similar features as the vertical velocity variance budget in Fig. 1. The buoyancy term in the cloud mass-flux budget (sampling criterion I_2 according to Table 1) has a negative value at the upper part of the cloud layer, whereas $w' \theta'_v$ is positive in this part. Therefore, the positive horizontal-mean buoyancy flux in this layer must be due to turbulence

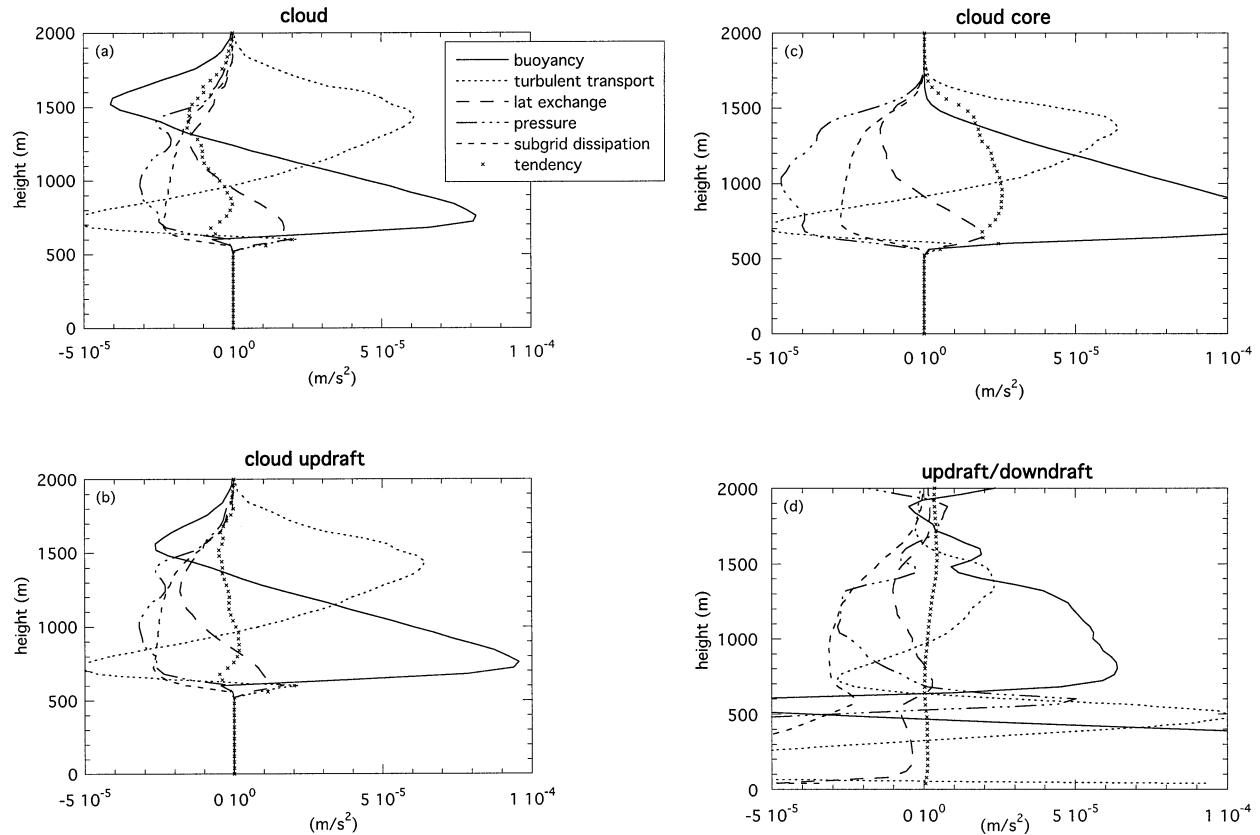


FIG. 3. Mass-flux budgets for the (a) cloud, (b) cloud updrafts, (c) cloud core, and (d) updraft-downdraft decomposition. The line styles are according to the legend shown in (a).

in the dry environment and to subplume perturbations within the cloud. By definition, the cloud core must have a positive buoyancy. Irrespective of the kind of decomposition applied, the turbulent transport term is an important production term for the convective mass flux in the upper part of the cloud layer. The conditionally sampled horizontal advection of vertical velocity, which formally represents the lateral exchange of mass flux, acts to produce mass flux at the lower part of the cloud layer and diminishes the mass flux above. The role of the pressure and subgrid flux terms are similar to the ones in the vertical velocity variance budget in the sense that they both tend to destroy mass flux. In that respect the subgrid flux term is analogous to the dissipation term in the vertical velocity variance budget, and this result might be somewhat controversial. Scaling considerations lead to the conclusion that dissipation by molecular viscosity can be neglected for motions on scales typical for cumulus convection and that it is only of importance at the largest wavenumbers of the velocity spectra—the Kolmogorov scales. The “dissipation” in the mass-flux budget, however, arises from the subgrid parameterization term (4) where the flux is parameterized as the product of an eddy viscosity times the local gradient. In the vertical velocity

variance equation it is exactly this term that causes the dissipation (see Table 2). However, the amount of the resolved kinetic energy that is lost is not dissipated into heat, but acts as a production term in the prognostic equation for the subgrid TKE equation, and therefore the subgrid term can be interpreted as a mechanism to convert resolved motions into subgrid perturbations. Hence, in the mass-flux budgets the subgrid parameterization term removes vertical momentum from the sampled eddies to feed the turbulent motions of small-scale eddies that have sizes smaller than the grid size of the LES.

For the cloud core decomposition the total tendency of the mass flux including the boundary terms is significant. Since the cloud core mass flux hardly changes with time, $\partial M_c / \partial t \approx 0$, this implies that the time tendency of the mass flux is predominantly due to the Leibniz boundary term in (15). It means that some of the cloud parcels that are accelerated disappear from the cloud sample at the next computational time step by detrainment to its surrounding environment.

b. The vertical velocity budget

The convective available potential energy (CAPE) can be written as

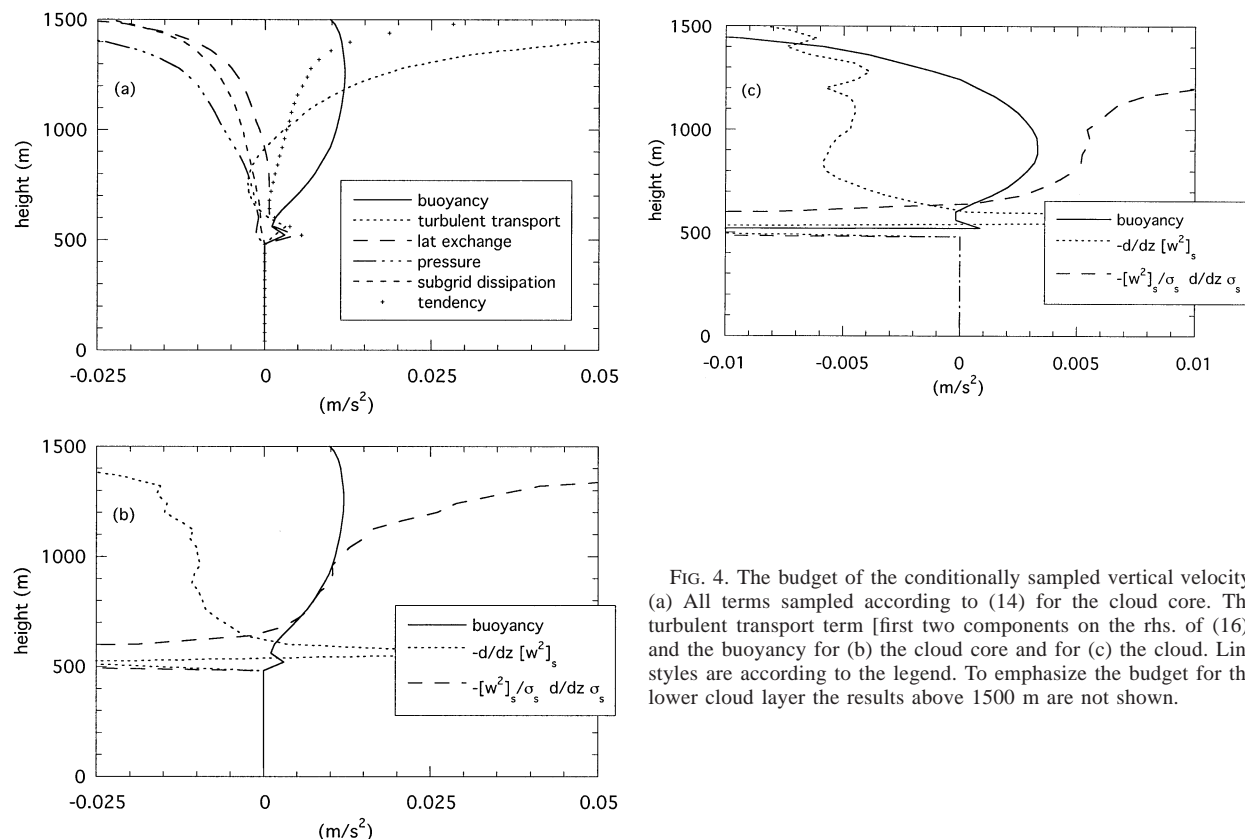


FIG. 4. The budget of the conditionally sampled vertical velocity. (a) All terms sampled according to (14) for the cloud core. The turbulent transport term [first two components on the rhs. of (16)] and the buoyancy for (b) the cloud core and for (c) the cloud. Line styles are according to the legend. To emphasize the budget for the lower cloud layer the results above 1500 m are not shown.

$$\text{CAPE} = \int_{z_{\text{LFC}}}^{z_{\text{LOC}}} \frac{g}{\theta_0} (\theta_{v,s} - \theta_{v,e}) dz, \quad (32)$$

where z_{LFC} represents the level of free convection and z_{LOC} the limit of convection, that is, the level above which the cloud is negatively buoyant with respect to its environment. CAPE is often used to estimate the characteristic vertical velocity scale (w_{CAPE}) in shallow cumulus clouds (Stull 1988),

$$w_{\text{CAPE}} = (2\text{CAPE})^{1/2}, \quad (33)$$

in which it is assumed that all the potential energy is converted into kinetic energy.

Figure 4a shows the budget for the conditionally sampled cloud core vertical velocity according to (14). One particularly striking feature is that the transport term has a small negative value in the lower 400 m of the cloud layer and becomes positive above. If the turbulent transport and the buoyancy would be the sole terms giving a contribution to the prognostic sampled vertical velocity equation (14), then the turbulent transport term should have been the negative of the buoyancy at every height:

$$\frac{g}{\theta_0} (\theta_{v,s} - \bar{\theta}_v) = \left[\frac{\partial w^2}{\partial z} \right]_s. \quad (34)$$

Obviously, this is an unrealistic assumption. Figure 4b

depicts the buoyancy and the first two components of the turbulent transport term on the rhs of (16) separately for the cloud core. It can be seen that the term including the vertical derivative of σ_s is responsible for the positive value of the total turbulent transport term. The vertical derivative of the sampled vertical velocity variance, $-\partial[w^2]_s/\partial z$, is negative throughout the cloud layer. Because the vertical gradient of the sampled vertical velocity variance is the largest negative term in the budget, one might be inclined to conclude the following CAPE formula is an acceptable zeroth-order approximation:

$$[w^2]_{s,z_{\text{LOC}}} = \text{CAPE}. \quad (35)$$

The results in Fig. 4a, however, indicate that this approximation is justified only because all the other terms roughly balance each other, rather than that they are negligibly small. For the cloud–environment decomposition we find from Fig. 4c that the buoyancy term in the middle of the cloud layer is about a factor of 2 smaller than the vertical derivative of the conditionally sampled vertical velocity variance, indicating that the ratio between the two terms in (35) critically depends on the sampling criterion.

Note that (35) includes the conditionally sampled vertical velocity variance at the limit of convection, whereas (33) considers a vertical velocity scale. If one assumes

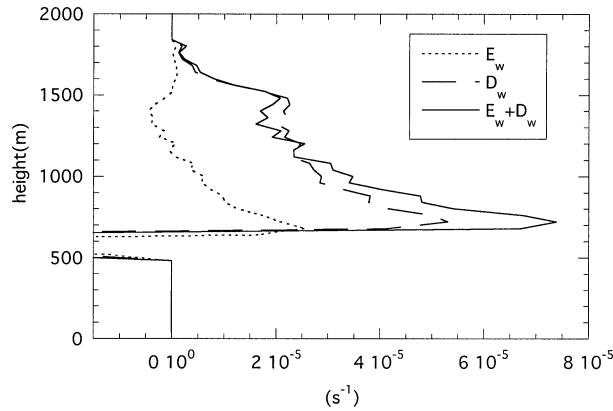


FIG. 5. Lateral entrainment (E_w) and detrainment (D_w) rates, and their sum, for the vertical velocities sampled in the cloud core.

a top-hat distribution for the vertical velocity, $[w^2]_{s,z_{\text{LOC}}} = w_{\text{CAPE}}^2$, then (33) and (35) are identical except for a factor of 2. The factor 2 depends on whether the advection terms in the vertical momentum equation are expressed in an advective or in a flux form as in Eq. (2). In the latter case the continuity equation multiplied by the vertical velocity has been added to the vertical momentum equation, which explains why expression (35) is without the factor 2. Because the horizontal advection terms are also modified by expressing them in a flux form, the difference is incorporated into the horizontal momentum flux divergence term, which has been neglected in the derivation of (35).

c. Entrainment and detrainment

The diagnosed entrainment and detrainment rates for the cloud core decomposition are shown in Fig. 5. The entrainment and detrainment rates for the vertical velocity have slightly smaller values compared to the ones found for conserved variables by Siebesma and Cuijpers

(1995). The entrainment rate E_w becomes negative above 1000 m. For other sampling criteria we also find negative values for E_w . However, one should be reminded that the net effect of lateral mixing in the vertical velocity variance budget equation (26) is given by $-(E_w + D_w)(w_s - w_e)^2$. If $(E_w + D_w) > 0$, this term acts to dissipate the vertical velocity variance, which is the case for the bulk of the cloud layer except in a shallow layer near the cloud base. As was noted by Petersen et al. (1999), the approach to compute the lateral entrainment and detrainment rates as a residual term of (22) does not guarantee them to be positive. Moreover, they remarked that the diagnosed lateral mixing rates may be scalar dependent, as is the case for the momentum and the conserved scalar equations. This seems to violate the concept that $D(E)$ represent the lateral mass exchange from the sampled cloud (environment) into the environment (sampled cloud), which rate is uniquely determined from the conditionally sampled continuity equation for mass. The E_w and D_w are the effective bulk entrainment and detrainment rates that would make the vertical velocity budgets balance after the assumption that the entrained or detrained air properties are the averaged conditionally sampled air properties. The obtained results for E_w and D_w should therefore be rather interpreted as tuned, reciprocal timescales for the conditionally sampled vertical velocity equation. Note that in higher-order closure modeling it is not unusual to use different time or length scales (Mellor and Yamada 1982).

d. The vertical velocity variance budget

Figure 6 presents the vertical velocity variance budget in the mass-flux approach (26) for the cloud core. The dissipation is computed with the values for E_w and D_w shown in Fig. 5. Although they are not identical, the physical interpretation of the budget is similar to the

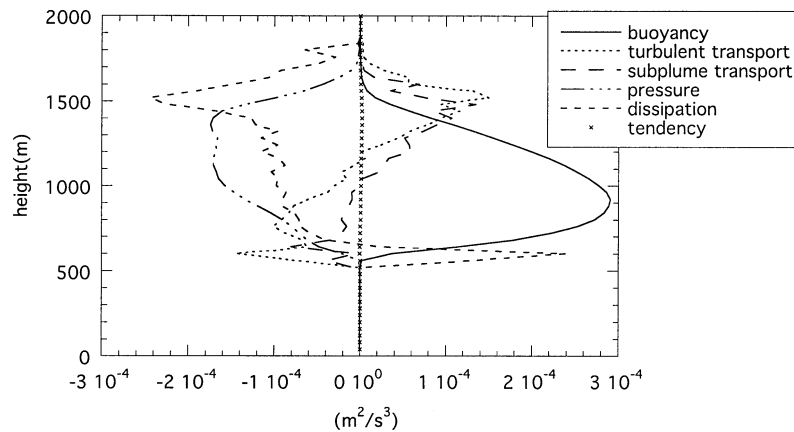


FIG. 6. The cloud core vertical velocity variance budget in the mass-flux approach according to (26); the dissipation is represented by the term, $-(E_w + D_w)(w_s - w_e)^2$. Line styles are according to the legend.

vertical velocity variance budget. Since cloud core points are partly selected on the basis of a positive buoyancy excess, the buoyancy flux is producing vertical velocity variance throughout the cloud layer. As a consequence, the cloud core decomposition cannot represent overshooting clouds that rise due to their inertia despite a negative buoyancy excess. The turbulent transport and the subplume contribution are both important in the redistribution of vertical velocity variance from the lower part to the upper part of the cumulus cloud layer. A similar result was found by Young (1988b) and Schumann and Moeng (1991a) from an analysis of updrafts and downdrafts in the clear convective boundary layer. The turbulent transport term was found to redistribute vertical momentum generated in the lower part of the mixed layer into the upper part of the mixed layer. The subplume transport was alike the turbulent transport but at a smaller rate. The pressure term and the dissipation act to destroy the vertical velocity variance. The cloud core budget resembles the Reynolds-averaged vertical velocity variance budget the most in comparison to other sampling criteria. In the next section this will be illustrated from a discussion of the virtual potential temperature flux in the mass-flux approach.

5. Thermodynamic characteristics of the conditionally sampled cumulus clouds

a. The conditionally sampled virtual potential temperature flux and vertical velocity variance

Figure 7 shows the conditionally sampled virtual potential temperature flux $\sigma_s[w'\theta'_v]_s$ and vertical velocity variance $\sigma_s[w'w']_s$. The vertical flux of the virtual potential temperature is mainly determined by in-cloud turbulence. Turbulent vertical motions in the cloud and in the environment contribute nearly equally to the vertical velocity variance. Probably, a good deal of the vertical velocity variance in the dry environment can be attributed to gravity waves, which can develop owing to the conditionally unstable stratification in the cloud layer.

Since θ_v is not conserved when evaporation/condensation of liquid water occurs, it is questionable how well the mass-flux approximation can represent the Reynolds-averaged statistics. In Fig. 8 its validity is checked for both the virtual potential temperature flux and the vertical velocity variance. For the cloud core decomposition the virtual temperature flux in the mass-flux approach $M_c(\theta_{v,s} - \theta_{v,c})$ is only a fraction smaller than the Reynolds-averaged flux $\overline{w'\theta'_v}$, but the difference between the Reynolds-averaged and mass-flux approximation is larger for the cloud updraft and cloud decomposition. This can be explained by the fact that for the cloud core decomposition parcels with a negative virtual potential temperature perturbation are filtered out, whereas $\theta_{v,s}$ for the cloud/cloud updraft is lowered by the inclusion of such parcels. The vertical velocity var-

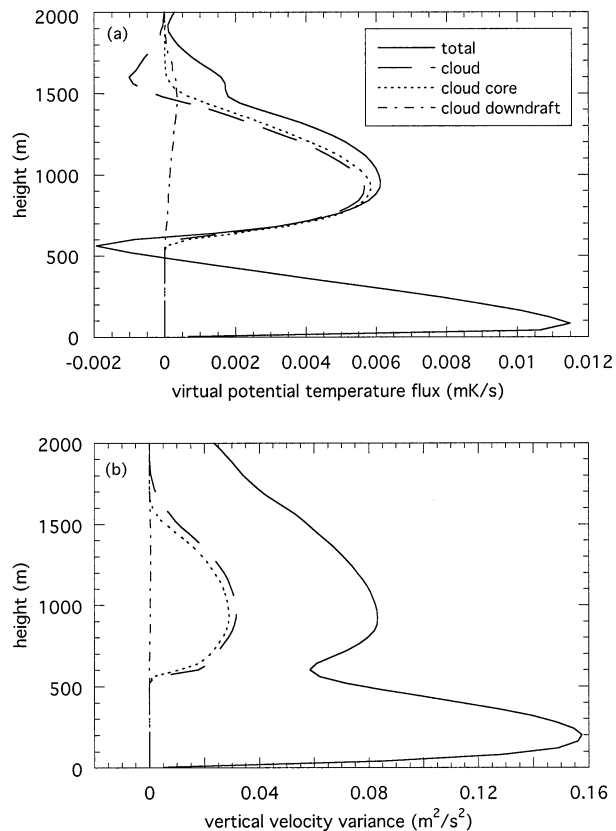


FIG. 7. Conditionally sampled (a) virtual potential temperature flux ($\sigma_s[w'\theta'_v]_s$) and (b) vertical velocity variance ($\sigma_s[w'w']_s$). Note that only the resolved parts of the fluxes and variances have been conditionally sampled. The total resolved slab-averaged values of $\overline{w'\theta'_v}$ and $\overline{w'w'}$ are also shown for reference (solid lines). The line styles are according to the legend shown in (a).

iance is not very well represented by any of the applied cloud decompositions, either. This can be expected because a good deal of the vertical velocity variance is found outside the clouds (see Fig. 7b).

b. Evaporative cooling and the generation of downdrafts

Figure 9 shows the conditionally sampled area fraction, vertical velocity, the virtual potential temperature, the total water content, and the potential temperature for the cloud updraft and downdraft and the cloud core. The cloud downdraft fraction is rather small throughout the whole cloud layer. However, as is shown in Fig. 10, its fraction of the total cloud cover increases from about 4% at 600 m to more than 20% above 1200 m. The average minimum vertical velocity of the cloud downdrafts decreases with height to about -0.7 m s^{-1} at 1500 m, where the cloud downdrafts have a significantly lower virtual potential temperature than the horizontal slab-mean value (about -1 K). The absolute value of this number is more than a factor of 2 larger than the max-

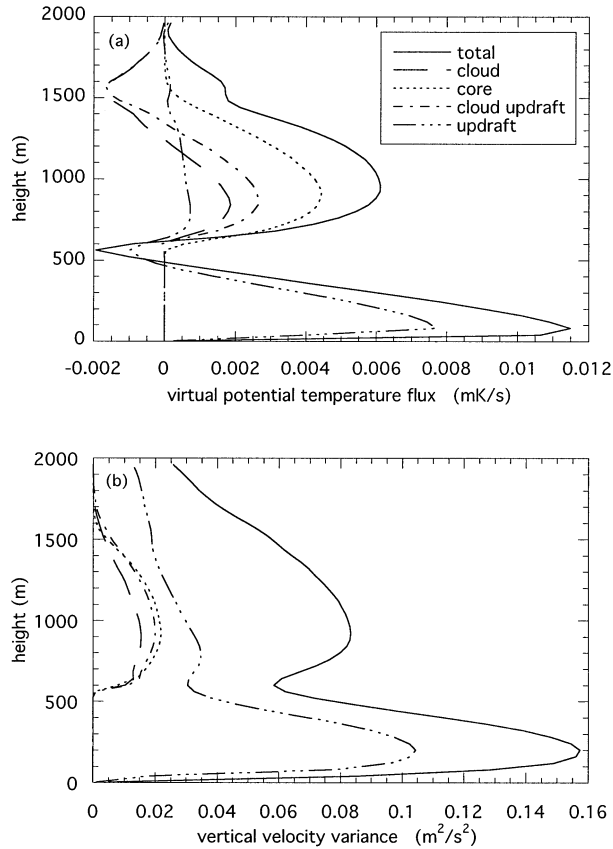


FIG. 8. (a) Virtual potential temperature flux, $M_c(\theta_{v,s} - \theta_{v,e})$, and (b) vertical velocity variance, $M_c(w'_s - w'_e)$, in the mass-flux approach. The total resolved slab-averaged values for $w'\theta'_v$ and $w'w'$ are also shown for reference (solid lines).

imum difference for the cloud core, which is about +0.4 K, where it should be noted that a positive buoyancy excess is one of the criteria that defines the cloud core.

The role of mixing of dry environmental air with cloudy air at either the lateral sides of the cloud or the cloud top has been suggested to be a major mechanism leading to cold downdrafts (Raymond and Blyth 1986; Kain and Fritsch 1990; Taylor and Baker 1991; Jonas 1990; Blyth 1993). These downdrafts have been observed both within and just outside the cloud. To evaluate the possible role of lateral mixing on the formation of cold downdrafts we have computed the minimum virtual potential temperature that can be obtained by mixing cloudy and environmental air. It must be noted that, although we refer to lateral mixing in this case, the cloud ensemble includes clouds in all possible stages, such as growing clouds which may mix with dry air at their tops. For a mixed parcel that contains a mixture of cloudy and environmental air with mean properties ψ_s and ψ_e , respectively, the value of an arbitrary conserved variable ψ_m is given by

$$\psi_m = \chi\psi_e + (1 - \chi)\psi_s, \quad (36)$$

where $\chi = m_e/(m_e + m_s)$ is the mixing fraction, m_e and m_s are the masses of a parcel from the surrounding cloud environment and cloud, respectively. If dry air is gradually mixed with cloudy air some cooling will take place by evaporation of liquid water (Randall 1980; Deardorff 1980; Duynkerke 1993).

The effect of evaporative cooling is depicted in Fig. 11. It shows how the virtual potential temperature of the mixed parcel relative to the environment changes as a function of the mixing fraction χ . For the critical mixing fraction χ_* all the liquid water is just evaporated and the maximum amount of cooling is obtained. In the absence of liquid water, the virtual potential temperature can be considered to be a conserved variable, and the effect of mixing on the mixed parcel is a linear function of χ as described by Eq. (36). Note that the mixing fraction for which the mixed parcel is just neutrally buoyant is even smaller than the critical mixing fraction, and is about $\chi \approx 0.1$ for the example shown.

Figure 12 shows the critical mixing fractions and the associated minimum virtual potential temperature of a mixed parcel with respect to the horizontal slab mean as a function of height for the cloud and cloud core decomposition. A mixing fraction $\chi < 0.5$ is needed to evaporate all the cloud core liquid water. The critical mixing fraction has a slightly smaller value for the cloud–environment decomposition since the mean sampled cloud liquid water content is lower than for the cloud core. However, irrespective the kind of cloud decomposition made the minimum virtual potential temperature that can be obtained by lateral mixing is approximately the same. Furthermore, the minimum virtual potential temperature is smaller than the horizontal slab mean value at every height in the cloud layer. This can be easily explained by the fact that cloudy air has its primary origin in the subcloud layer, which has a lower virtual potential temperature ($\theta_{v,\text{subcloud}}$) than the cloud layer $\bar{\theta}_v(z)$. For example, Fig. 12b also shows the virtual potential temperature difference between a dry undiluted parcel starting off from cloud base ($z = 500$ m) and the mean vertical profile. After mixing between air from the subcloud layer and the conditionally unstable layer the virtual potential temperature of a (just) unsaturated mixed parcel ($\theta_{v,m}$) is given by the mixing equation for conserved variables (36) such that $\theta_{v,m}$ is constrained by

$$\theta_{v,\text{subcloud}} \leq \theta_{v,m} \leq \bar{\theta}_v(z). \quad (37)$$

In other words, Eq. (37) states that any unsaturated, mixed air parcel that has been detrained from the cloud will always have a smaller virtual potential temperature than the horizontal slab mean value at the level where it is detrained. It means that lateral mixing counteracts the latent heat release in the cumulus cloud and even causes the generation of cold air parcels that can sink and subsequently generate turbulent kinetic energy in the environment of the cumuli. A similar conclusion is

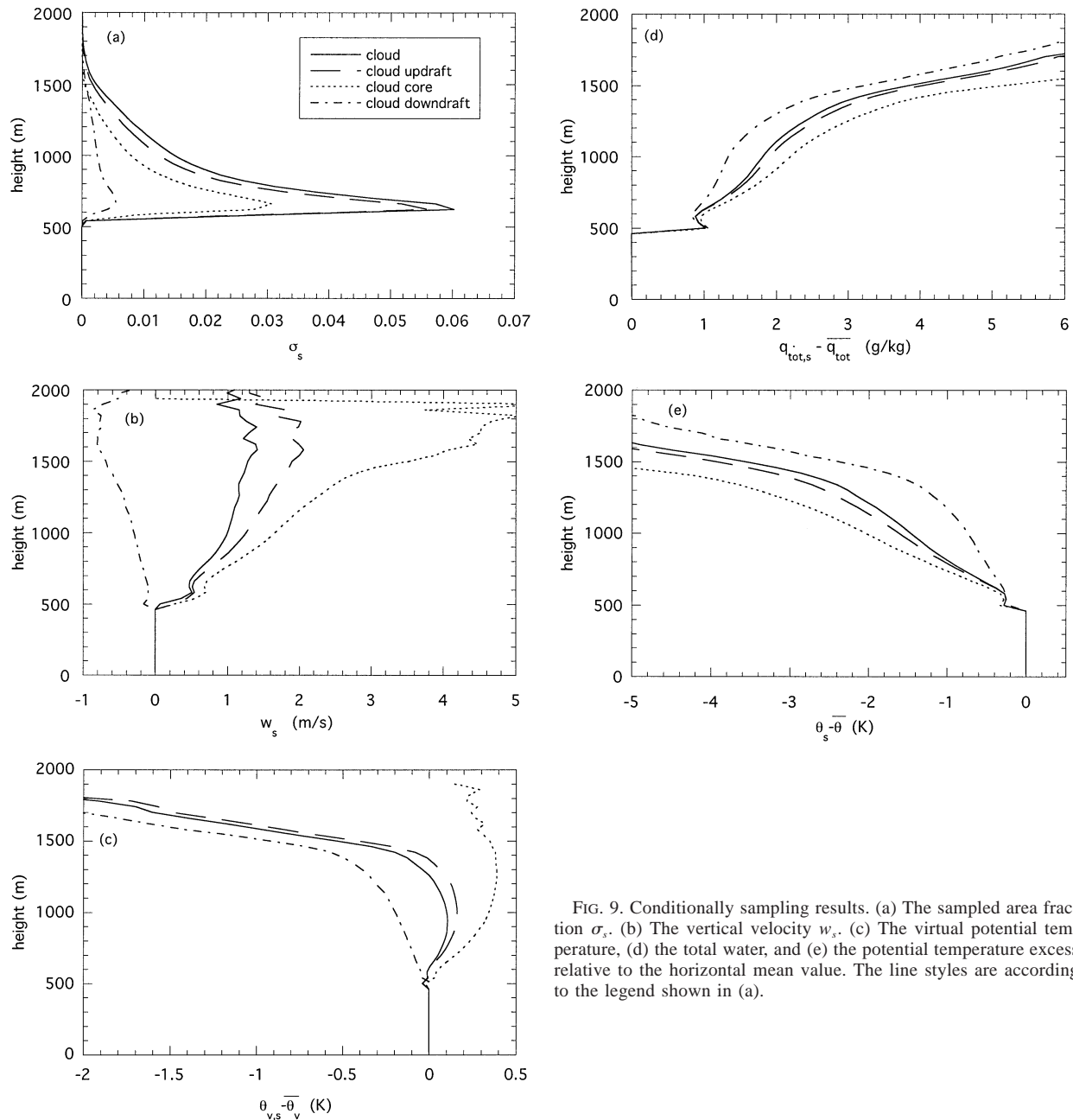


FIG. 9. Conditionally sampling results. (a) The sampled area fraction σ_s . (b) The vertical velocity w_s . (c) The virtual potential temperature, (d) the total water, and (e) the potential temperature excess relative to the horizontal mean value. The line styles are according to the legend shown in (a).

drawn by Rods (2001) from an analysis of aircraft observations made above Florida.

Note that, if the mean potential temperature (Fig. 9e) of the cloud is less than in the environment, this should also be the case for the temperature. It implies that if one measures a lower average temperature in a cumulus cloud from an instrumented aircraft this may be due to mixing and does not necessarily mean that the instrument is affected by wetting and a subsequent evaporative cooling.

Summarizing, the results presented in this section suggest that the top-hat approach for the vertical ve-

locity tendency equation does not work as satisfactorily as for a conserved variable. The reason why this is the case is possibly best illustrated by Fig. 9. If one compares the conditionally sampled total water contents for different criteria, it is clear that they differ slightly, but nevertheless they all differ systematically from the environment. Because q_i is a conserved variable, mixing causes q_i to change according to (36) and as depicted by the linear mixing line in Fig. 11. The sign of the difference ($q_{i,s} - q_{i,e}$) is therefore conserved. However, this is not the case for the virtual potential temperature θ_v . Figure 11 shows that even for a small mixing frac-

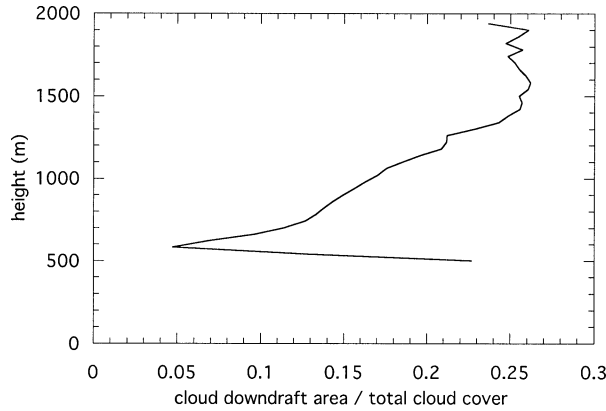


FIG. 10. The cloud downdraft area fraction divided by the total cloud area fraction.

tion, $(\theta_{v,s} - \theta_{v,e})$ becomes negative. Since the buoyancy is the primary forcing term for the vertical velocity tendency, a negative buoyancy will cause the cloud updrafts to slow down and to become either cloud or dry negatively buoyant downdrafts.

6. Summary and conclusions

The dynamics of shallow cumulus have been investigated by means of a large eddy simulation based on the BOMEX observations. By conditionally sampling on the presence of liquid water as an indicator function a distinction between clouds and environment could be made, while additional sampling criteria were used to select cloud downdrafts, cloud updrafts, and cloud cores (a positive vertical velocity and buoyancy excess).

Prognostic equations for the conditionally sampled vertical velocity, the mass flux, and the vertical velocity variance in the mass-flux approach were derived by conditionally sampling the prognostic vertical velocity equation. From an analysis of the vertical velocity variance budget the following dynamical picture emerges. The vertical velocity variance in the cloud layer is primarily driven by a positive buoyancy flux due to condensational heating in the clouds. The turbulent transport term redistributes vertical velocity variance from the lower to the upper part of the cloud layer. The pressure term and the subgrid parameterization term are both acting to destroy the vertical velocity variance. The pressure redistributes vertical velocity into horizontal directions, while the subgrid term removes momentum from the resolved flow to feed turbulent subgrid eddies, which have typical length scales that are smaller than the grid size of the LES model. Since the equations for vertical velocity variance and the mass flux arise from the same vertical velocity equation their budgets appear qualitatively similar. The mass-flux budgets for different sampling criteria are not identical. This means that, for example, if one develops a parameterization for the pressure term to be used in a prognostic mass-flux equation,

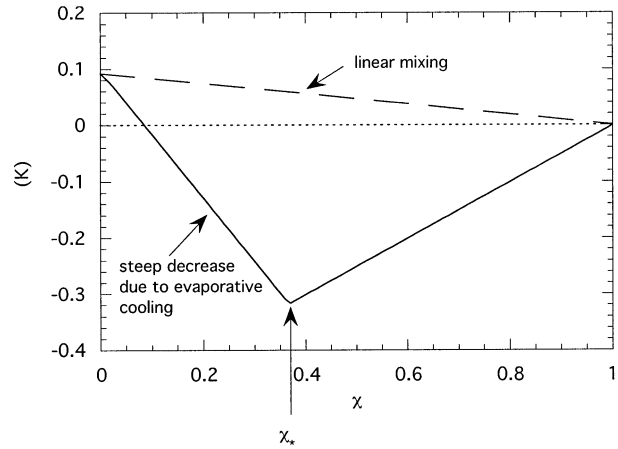


FIG. 11. Example of a mixing diagram showing how the virtual potential temperature depends on the mixing fraction between cloudy and dry environmental air. The diagram is computed from data at 1020 m for the cloud–environment decomposition.

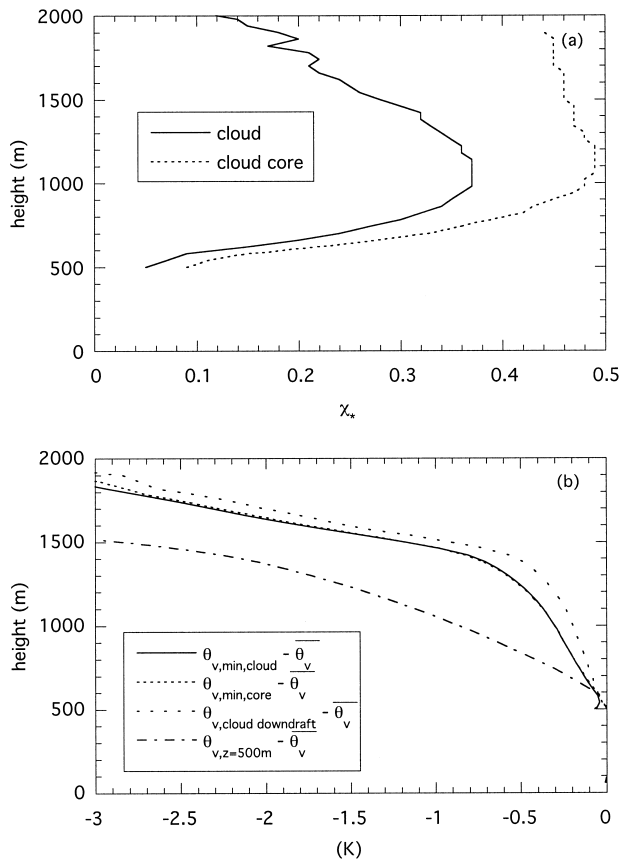


FIG. 12. (a) The critical mixing fraction χ_* as function of height. (b) The minimum virtual potential temperature of the mixed parcel ($\theta_{v,\min}$) that can be obtained after mixing cloud (core) and environmental air. In addition, the virtual potential temperature of the cloud downdrafts, and the virtual potential temperature of a rising undiluted dry air parcel starting from $z = 500$ m (dry-adiabatic ascent) are shown. The horizontal slab mean virtual potential temperature has been subtracted from all profiles. The line styles are according to the legend.

the precise formulation of it depends on the particular definition one uses for the cloud.

Cloud downdrafts were found to occupy up to about 20% of the total cloud cover in the upper part of the cloud. Because the cloud downdrafts have a negative virtual potential temperature with respect to the horizontal slab mean, this suggests that they were formed by mixing with dry environmental air giving rise to evaporative cooling. The occurrence of downdrafts and negatively buoyant parcels in the cloud has an important implication for mass-flux modeling. Whereas the vertical flux of a generic conserved variable ψ is well described by the mass-flux approach, it gives less satisfactory results for the virtual potential temperature flux and vertical velocity variance. Therefore, to obtain these second-order moments from a top-hat approach, it is necessary to include the effect of the subplume perturbations if one aims to get results that are identical to the Reynolds-averaged ones (Petersen et al. 1999; Lappen and Randall 2001b; Wang and Stevens 2000).

Although the cloud core decomposition provides the best representation for the vertical velocity variance and the vertical flux of conserved variables, it has two major disadvantages. First, it cannot represent overshooting clouds that rise due to their inertia despite a negative buoyancy excess. Second, the cloud core area fraction is not equal to the cloud area fraction that is needed for the computation of the radiative transfer. These drawbacks can be overcome by applying the cloud criterion I_2 (Table 1). Also, Lappen and Randall (2001b,c) showed that the BOMEX case can be reasonably well simulated by the updraft–downdraft decomposition. However, the cloud fraction needs to be prognosed separately in this approach. The updraft–downdraft decomposition also facilitates the simulation of convection in the clear convective boundary layer and in stratocumulus-topped boundary layers. The vertical velocity budgets for these types of boundary layers have been discussed by Young (1988b) and Schumann and Moeng (1991a).

In the classical view a cumulus cloud is sketched as a turbulent updraft surrounded by laminar compensating subsidence motions. However, a somewhat more complicated picture emerges from the LES results. First of all, the vertical velocity variance, which is a typical indicator of the turbulence intensity, is about as large in the cloud as in the dry environment. Probably, a good deal of the vertical velocity variance in the dry environment can be attributed to gravity waves, which can develop owing to the conditionally unstable stratification in the cloud layer. The effect of the turbulent, subplume motions in the dry environment of the cloud on the vertical transport of quantities like total water or the liquid water potential temperature is, however, very small.

In a model in which the entrainment and detrainment rates are prescribed and in which the continuity equation for mass (23) is used to determine the mass flux, the

vertical mass-flux gradient is fully constrained. The advantage of any prognostic equation for the vertical velocity in the mass-flux approach is that it links the thermodynamic state of the atmosphere to the dynamics by the buoyancy term. Kain and Fritsch (1990) demonstrated from a model simulation that the vertical mass-flux profile depended on the ambient moisture content and the convective available potential energy. As an example, they found that, if the relative humidity in the cloud layer was increased from 50% to 90%, the updraft mass-flux maximum shifted from the lower part to the upper part of the cloud layer. It is therefore tempting to extend the study presented in this paper by exploring the budgets for the conditionally sampled vertical velocities for a wide variety of boundary conditions.

Acknowledgments. This work was supported by NASA Grant NAG1-2072. We thank Herve Grenier for the many stimulating discussions and Peter Duynkerke for giving useful comments on an earlier version of the manuscript. We would also like to thank three anonymous reviewers for their helpful suggestions.

REFERENCES

- Arakawa, A., and W. H. Schubert, 1974: Interaction of a cumulus cloud ensemble with the large-scale environment: Part I. *J. Atmos. Sci.*, **31**, 674–701.
- Asai, T., and A. Kasahara, 1967: A theoretical study of the compensating downward motions associated with cumulus clouds. *J. Atmos. Sci.*, **24**, 487–496.
- Blyth, A. M., 1993: Entrainment in cumulus clouds. *J. Appl. Meteor.*, **32**, 626–641.
- Cotton, W. R., 1975: On the parameterization of turbulent transport in cumulus clouds. *J. Atmos. Sci.*, **32**, 548–564.
- Cuijpers, J. W. M., 1994: Large-eddy simulation of cumulus convection. Ph.D. thesis, Technical University Delft, Delft, Netherlands, 150 pp.
- , P. G. Duynkerke, and F. T. M. Nieuwstadt, 1996: Analyses of variance and flux budgets in cumulus-topped boundary layers. *Atmos. Res.*, **40**, 307–337.
- Deardorff, J. W., 1973: Three-dimensional numerical modeling of the planetary boundary layer. *Workshop on Micrometeorology*, D. A. Haugen, Ed., Amer. Meteor. Soc., 271–311.
- , 1980: Cloud-top entrainment instability. *J. Atmos. Sci.*, **37**, 131–147.
- de Laat, A. T. J., and P. G. Duynkerke, 1998: Analysis of astrotocumulus observational data using a mass-flux approach. *Bound.-Layer Meteor.*, **86**, 63–87.
- de Roode, S. R., P. G. Duynkerke, and A. P. Siebesma, 2000: Analogies between mass-flux and Reynolds-averaged equations. *J. Atmos. Sci.*, **57**, 1585–1598.
- Duynkerke, P. G., 1993: The stability of cloud top with regard to entrainment: Amendment of the theory of cloud-top entrainment instability. *J. Atmos. Sci.*, **50**, 495–502.
- Grant, A. L. M., and A. R. Brown, 1999: A similarity hypothesis for shallow-cumulus transports. *Quart. J. Roy. Meteor. Soc.*, **125**, 1913–1936.
- Holton, J. R., 1973: A one-dimensional cumulus model including pressure perturbations. *Mon. Wea. Rev.*, **101**, 201–205.
- Jonas, P. R., 1990: Observations of cumulus cloud entrainment. *Atmos. Res.*, **25**, 105–127.
- Kain, J. S., and J. M. Fritsch, 1990: A one-dimensional entraining/detraining plume model and its application in convective parameterization. *J. Atmos. Sci.*, **47**, 2784–2802.

- Lappen, C.-L., and D. A. Randall, 2001a: Toward a unified parameterization of the boundary layer and moist convection. Part I: A new type of mass-flux model. *J. Atmos. Sci.*, **58**, 2021–2036.
- , and —, 2001b: Toward a unified parameterization of the boundary layer and moist convection. Part II: Lateral mass exchanges and subplume-scale fluxes. *J. Atmos. Sci.*, **58**, 2037–2051.
- , and —, 2001c: Toward a unified parameterization of the boundary layer and moist convection. Part III: Simulations of clear and cloudy convection. *J. Atmos. Sci.*, **58**, 2052–2072.
- Mellor, G. L., and T. Yamada, 1982: Development of a turbulence closure model for geophysical fluid problems. *Rev. Geophys. Space Phys.*, **20**, 851–875.
- Nitta, T., 1975: Observational determination of cloud mass flux distributions. *J. Atmos. Sci.*, **32**, 73–91.
- Petersen, A. C., C. Beets, H. van Dop, P. G. Duynkerke, and A. P. Siebesma, 1999: Mass-flux characteristics of reactive scalars in the convective boundary layer. *J. Atmos. Sci.*, **56**, 37–56.
- Raga, G. B., J. B. Jensen, and M. B. Baker, 1990: Characteristics of cumulus band clouds off the coast of Hawaii. *J. Atmos. Sci.*, **47**, 338–355.
- Randall, D. A., 1980: Conditional instability of the first kind upside down. *J. Atmos. Sci.*, **37**, 125–130.
- , Q. Shao, and C.-H. Moeng, 1992: A second-order bulk boundary-layer model. *J. Atmos. Sci.*, **49**, 1903–1923.
- Raymond, D. J., and A. M. Blyth, 1986: A stochastic mixing model for nonprecipitating cumulus clouds. *J. Atmos. Sci.*, **43**, 2708–2718.
- Rodts, S. M. A., 2001: Shallow cumulus dynamics: Observations and parameterizations. M.S. thesis, Utrecht University, Utrecht, Netherlands, 78 pp.
- Schumann, U., and C.-H. Moeng, 1991a: Plume budgets in clear and cloudy convective boundary layers. *J. Atmos. Sci.*, **48**, 1758–1770.
- , and —, 1991b: Plume fluxes in clear and cloudy convective boundary layers. *J. Atmos. Sci.*, **48**, 1746–1757.
- Siebesma, A. P., 1998: Shallow cumulus convection. *Buoyant Convection in Geophysical Flows*, E. J. Plate et al., Eds., Vol. 513, Kluwer Academic, 441–486.
- , and J. W. M. Cuijpers, 1995: Evaluation of parametric assumptions for shallow cumulus convection. *J. Atmos. Sci.*, **52**, 650–666.
- , and A. A. M. Holtslag, 1996: Model impacts of entrainment and detrainment rates in shallow cumulus convection. *J. Atmos. Sci.*, **53**, 2354–2364.
- Stevens, B., and Coauthors, 2001: Trade-wind cumuli under a strong inversion. *J. Atmos. Sci.*, **58**, 1870–1891.
- Stommel, H., 1947: Entrainment of air into a cumulus cloud. *J. Meteor.*, **4**, 91–94.
- Stull, R. B., 1988: *An Introduction to Boundary Layer Meteorology*. Kluwer Academic, 666 pp.
- Taylor, G. R., and M. B. Baker, 1991: Entrainment and detrainment in cumulus clouds. *J. Atmos. Sci.*, **48**, 112–121.
- Tiedtke, M., 1989: A comprehensive mass flux scheme for cumulus parameterization in large-scale models. *Mon. Wea. Rev.*, **117**, 1779–1800.
- VanZanten, M. C., 2000: Entrainment processes in stratocumulus. Ph.D. thesis, Utrecht University, Utrecht, Netherlands, 139 pp.
- Wang, S., and B. Stevens, 2000: Top-hat representation of turbulence statistics in cloud-topped boundary layers: A large-eddy simulation study. *J. Atmos. Sci.*, **57**, 423–441.
- Wyngaard, J. C., and C.-H. Moeng, 1992: Parameterizing turbulent diffusion through the joint-probability density. *Bound.-Layer Meteor.*, **60**, 1–13.
- Young, G. S., 1988a: Turbulence structure of the convective boundary layer. Part II: Phoenix aircraft observations of thermals and their environment. *J. Atmos. Sci.*, **45**, 727–735.
- , 1988b: Turbulence structure of the convective boundary layer. Part III: The vertical velocity budgets of thermals and their environment. *J. Atmos. Sci.*, **45**, 2039–2049.